

## Profiles of Ion Temperature and Neutral Density from the Simulation of Charge Exchange Measurements and Additional Experimental Data.

J. Stober, D. P. Coster, H.-U. Fahrbach, R. Fischer, G. Haas, W. Herrmann;  
O. Kardaun, A. Khutoretsky †, S. de Peña Hempel, D. Reiter‡, R. Schneider,  
H. Verbeek, the ASDEX-Upgrade team, and the NBI team

Max-Planck-Institut für Plasma-Physik, EURATOM-Association,  
D-85748 Garching, Germany

† RRC "Kurchatov-Institute", 123182, Moscow, Russia

‡ IPP, Forschungszentrum Jülich GmbH, EURATOM-Association,  
D-52425 Jülich, Germany

### 1 Introduction

At ASDEX-Upgrade a method to evaluate the ion temperature profile has been developed by fitting the measured energy spectra of the neutral hydrogen and deuterium fluxes varying the parameters of the  $T_i$  profile. Two detection principles are used to cover the extremely wide energy range [15 eV, 20 keV]. It turned out that a reasonable accuracy at the separatrix can only be obtained when measurements of the total neutral flux are included in the fit as well [1]. In addition to the  $T_i$  profile, the neutral density along the lines of sight and a spatially constant H/D-ratio are determined. The method can also be used during neutral beam injection (NBI) so that comparison with local  $T_i$  measurements from charge exchange recombination spectroscopy (CXRS) is possible. The results are also compared to classical logarithmic slope evaluation. Finally, the problem of the parameterization-dependent results is addressed and we present first results of a Bayesian approach to determine the necessary degree of regularization.

### 2 Experimental

The energy spectra of the neutral fluxes are measured with two methods. One is based on the reionization in a gas cell and an energy and mass separation of these ions in parallel electric and magnetic fields [2]. The lowest detectable energy is normally set to 500 eV. At ASDEX-Upgrade, there are two analysers of this type which both view the plasma from the outer midplane. One is fixed and views the plasma center (CXA I), the other is turnable to vary its poloidal and toroidal direction (CXA II). The other method is a time-of-flight analysis of the neutrals without isotope separation (LENA) [3]. Its energy range is between 15 eV and 1 keV. The total neutral flux is measured directly with an ion gauge at the outer vessel wall [4]. Additionally an  $H_\alpha$  measurement has been set up with a line of sight close to the one of LENA (horizontal, 20 cm above the magnetic axis). For the  $T_i$  evaluation further experimental data are used:  $n_e$  from interferometry combined with lithium beam,  $T_e$  from Thompson scattering or ECE, and the proton density from spectroscopy [5]. These quantities, as well as  $T_i$ , are assumed to be constant on flux surfaces.

### 3 Fitting procedure

To model the energy-resolved neutral fluxes  $S(E_0)$ , we assume that the velocity distribution of the ions has Maxwellian form:

$$S(E_0) = \frac{1}{2\pi^{3/2}} \int_0^L \langle \sigma_{cx} v_{rel} \rangle(x) \cdot n_0(x) \cdot n_i(x) \cdot \frac{\exp(-E_0/T_i(x))}{T_i^{3/2}(x)} \cdot E_0^{1/2} \cdot \exp\left(-\int_0^x \frac{ds}{\lambda_{tot}(s)}\right) dx$$

The neutral density is obtained with the EIRENE Monte-Carlo code [6], using only the experimental data and the  $T_i$  parameters of the corresponding iteration step as input for the plasma background. The positioning of an assumed source of neutrals at the outer plasma-facing structures (outer source), which is required by the code, turned out to be of minor importance. For very low densities inner-wall sources also play a role, but only for the central plasma. Volume recombination as source of neutrals must not be neglected. For the  $T_i$  profile a linear spline parameterization is used. Parameters to be fitted are the  $T_i$  values at the knots. Additional parameters are the spatially constant H/D-ratio and the strength of the outer source. We use a  $\chi^2$ -type minimization, which takes experimental errors into account. The number of time consuming neutral density calculations could be reduced to 3 or even less by a two step algorithm, which optimizes the parameter values for a fixed neutral density which is recalculated only in an outer loop. Parameter errors are estimated from the curvature at the minimum of  $\chi^2$ . In the following graphs error bars refer to one standard deviation.

### 4 Comparison with $T_i$ from other diagnostics

In the case of NBI heated plasmas, local  $T_i$ -data are available from CXRS [7] also. Figure 1 shows a comparison of the two methods. The agreement is quite good in this case.

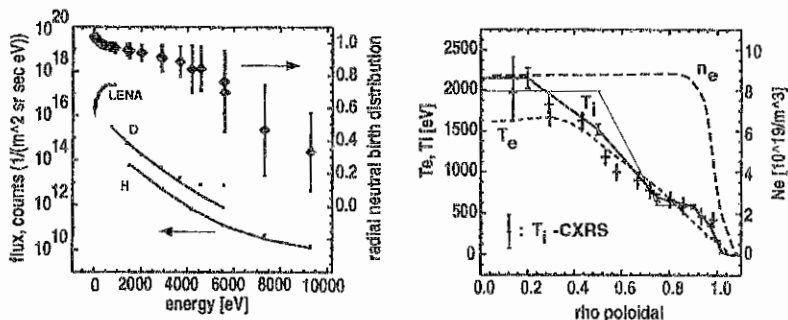


Figure 1: Analysis of a NBI-heated plasma ( $I_p = 1.0$  MA,  $B_t = -2.5$  T, 5 MW NBI).

Left: data with errors, fit (solid lines) and birth regions of the neutrals. Since deuterium is injected, this isotope deviates from the fit at higher energies. Only the 3 lowest points are used for  $\chi^2$ . Note that LENA data are given as uncalibrated count rates  $1/(m^2 sr sec)$  since isotopes cannot be separated. Right: temperature and density profiles. The thin solid line refers to a fit of the fluxes alone. The thick solid line is the result when the deviation from the CXRS values is included in  $\chi^2$  ( $\rho_{pol} = \sqrt{\frac{\Psi - \Psi_{axis}}{\Psi_{sep} - \Psi_{axis}}}$ ,  $\Psi = pol. Flux$ ).

Inclusion of the CXRS data improves the fit in the central plasma.

With the movable CXA II analyser, a series of similar shots was used to obtain the maximum  $T_i$  on different lines of sight from the logarithmic slope at high energies [8]. For the analysed scenario (ohmic,  $n_e = 3 \cdot 10^{19} m^{-3}$ ) the agreement was good and, as with CXRS, the fit could be improved including the additional data.

### 5 Ohmic density scan

As an application, an ohmic density scan is shown in figure 2:

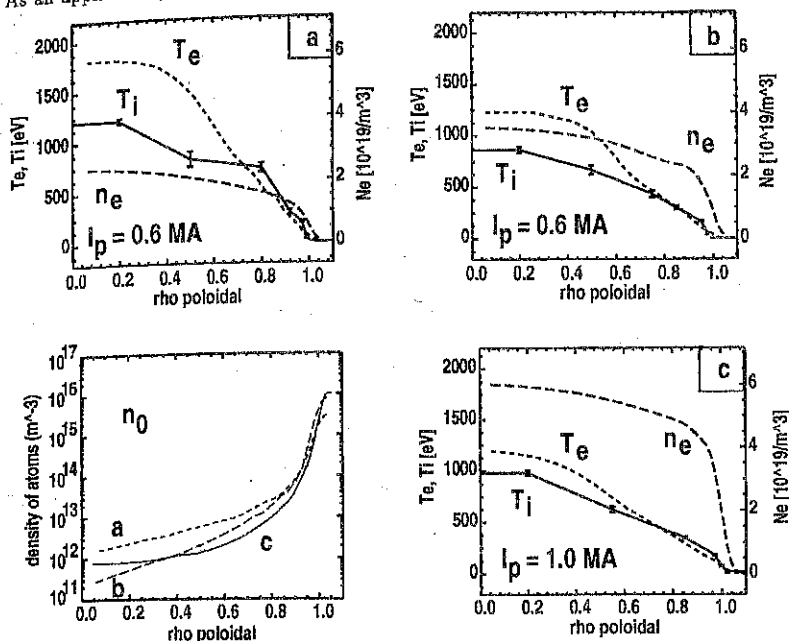


Figure 2: Comparison of ohmic discharges with different plasma densities.

The increased coupling between the primarily heated electrons and the ions with increased density leads to a decrease of the relative difference between  $T_e$  and  $T_i$ . In the analysed density range, the dominant source of neutrals in the center changes: In the low density case (a), only wall neutrals are important. As  $n_e$  increases (reduction of neutral mean free path),  $n_0$  decreases (b). Here, wall and volume sources are of equal importance for the center. With further increasing  $n_e$  (and nearly the same  $T_e$ ), the volume source dominates (c) and leads to a rather constant  $n_0$  over a wide radial range.

### 6 Bayesian Regularization

A problem of the procedure discussed so far, is the choice of the knot configuration of the linear spline for  $T_i$ . In practice, a trial configuration is accepted, if the resulting  $T_i$ -profile

has no oscillations and if  $\chi^2$  is reasonably low. Often several trials are necessary. Since several configurations are acceptable, the choice is somewhat arbitrary. Alternatively, one can choose "many" knots and use a regularization, for example by adding  $\lambda \int d\rho f(T^{(k)}(\rho))$  to the minimization functional. The choice of the weight  $\lambda$ , or even several weights for separate radial intervals, is often made manually (as is the choice of the intervals) and is to some extent arbitrary also.

Here, we present the results of a procedure that automatically determines its local degree of regularization combining an adaptive kernel method with Bayesian statistics [9]. The parameterization is  $T_i(\rho) = \sum_{j=1}^N h_j \cdot \exp(-\frac{(\rho-\xi_j)^2}{2b_j^2}) / \sqrt{2\pi} b_j$  with N "large enough" (here N = 37) and  $\xi_j$  fixed and spaced "narrowly enough". The regularization enters via a Bayesian prior distribution for  $\vec{b}$ :  $p(\vec{b}) = \Gamma(N_p/2) / (2\pi \sum_{j=1}^N b_j)^{N_p/2}$ ,  $N_p = \sum_{j=1}^N \frac{1}{b_j}$  being called the generalized dimension of the parameterization. The posterior distribution is analysed, and its maximum (MAP), its mean, and its variance are determined. As a first step, the method has been implemented with fixed neutral densities, that were obtained from the manual linear spline method. Figure 3 shows a comparison of both methods.

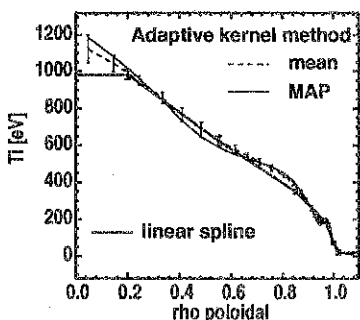


Figure 3: Comparison of the optimized linear spline (3rd trial, same as fig. 2c) with the result of the Bayesian adaptive kernel method. The error bars of the dashed curve represent the corresponding standard deviations of the posterior distribution. The  $T_i$  values and their errors agree well over a large radial range. The intuitive positioning of the knots seems to be sensible.

#### References

- [1] Stober J. et al., *Proc. of the 22nd EPS Conference on Controlled Fusion and Plasma Physics, Bournemouth, 1995*, **19C,III**, 249 (1995), EPS
- [2] Bartiromo et al., *Rev. Sci. Instrum.*, **58**, 788 (1987)
- [3] Verbeek H., *J. Phys.*, **E19**, 964 (1986),  
Verbeek H., Schiavi A., *IPP-Report*, **9/103**, (1994)
- [4] Haas G. et al., *J. Nucl. Mater.*, **121**, 151 (1984),  
Klepper C. C. et al., *J. Vac. Sci. Technol.*, **A 11**, 446 (1993)
- [5] Dux R. et al., *IPP-Report*, **10/1**, (1996)
- [6] Reiter D., *KFA Jülich reports, Jül-1947*, (1984), **Jül-2599**, (1992)
- [7] Boileau A., *Plasma Phys. Controlled Fusion*, **31**, 779, (1989)
- [8] Wagner F., *J. Vac. Sci. Technol.*, **20**, 1211 (1982)
- [9] Fischer R. et al., to be published